All-dielectric χ$^{(2)}$ metasurfaces: recent progress

Carlo Gigli[†] and Giuseppe Leo[†]*

Optical metasurfaces, i.e. arrays of nanoantennas with sub-wavelength size and separation, enable the manipulation of light-matter interactions in miniaturized optical components with no classical counterparts. Six decades after the first observation of the second harmonic generation (SHG) in bulk crystals, these devices are expected to break new ground in the field of nonlinear optics, shifting the focus from the phase matching approach achieved within long propagation distances to that of near-field resonances interplay in leaky nanocavities. Here we review the recent progress in SHG with all-dielectric metasurfaces. We discuss the most used technological platforms which underpinned such advances and analyze different SHG control approaches. We finally compare their performances with other well-established technologies, with the hope to delineate the current state-of-the-art and figure out a few scenarios in which these devices might soon offer unprecedented opportunities.

Introduction

The possibility to control, trap and shrink light down to the sub-wavelength scale[1] is one of the ultimate objectives of nanophotonics. At larger scales than light wavelength, the properties of the electromagnetic field can be harnessed via the electric permittivity ε_r and the magnetic permeability μ_r of the materials which host it. As such, the range of possible implementations in the visible and near-IR spectrum is restricted by the narrow window of accessible permittivities with natural dielectrics (typically $1 < \varepsilon_r < 16$). In order to overcome such limitations, both metals and dielectrics can be fabricated with a nano-structuration at the sub-wavelength scale, resulting in optical components with effective properties beyond those of bulk crystals, hence the name meta-optics. For example, single nanoantennas can act as optical transducers[2,3], confine light in deep sub-wavelength volumes[4,5] or control spontaneous emission[6] from single molecules[7] and quantum-dots[8], while nanopatterned 2D or 3D arrays can manipulate light propagation[9–11] and group velocity[12]. Such arrays correspond to metasurfaces, metamaterials and photonic crystals. The term metasurface, as a whole, includes both blazed binary gratings or high-contrast transmitarrays, designed to outperform conventional diffractive optical elements, and periodic arrangements of metallic or dielectric nanoresonators. In recent years, the latter have drawn the attention of the scientific community, especially due to the phenomenological richness of highly multi-mode Mie-type resonators. This unique feature emerged as an intriguing solution to induce non-trivial interference effects, which lead, among others, to the observation of Fano resonances[13–15], unidirectional scattering[16–18], anapole states[19], and bound states in the continuum[20–23] (BICs). Although metals proved attractive to obtain resonances with extremely small mode volumes[5], in some applications their

absorption losses can be a problem[24], and dielectric nanostructures[25] have progressively set in as a better-suited solution. This is the case, among others, of bio-sensing[26−28], quantum optics[29−31] and nonlinear devices[32]. Strong field confinement in photonic structures is an important ingredient for nonlinear optical generation to create sources of entangled photons[33], tunable cavities[34], and ultra-fast modulators[35−37]. In this context, nonlinear metasurfaces made of purely dielectric resonators appear as a promising alternative to already existing platforms, like nonlinear waveguides. This domain is evolving rapidly, and several reviews have already been published on the topic[38−41].

The present work aims at reviewing the recent advancements in the field of nonlinear all-dielectric metasurfaces operating in the visible/near-infrared (IR) window, with a particular focus on second harmonic generation (SHG). The manuscript is organized as follows: in Section *SHG in all-dielectric nanoantennas* we introduce the topic of nonlinear generation in Mie resonators, pointing out the main figures of merit for a high efficiency in non-Hermitian systems. Then, in Section *SHG in all-dielectric metasurfaces*, we overview the main approaches adopted in recent years to control or boost harmonic generation in metasurfaces. Finally, the conclusion in Section *Conclusion and outlook* provides a comparison with other existing technologies, outlining the current state-of-the-art and the possible perspectives in the near future.

SHG in all-dielectric nanoantennas

Historically, nonlinear generation at the nanoscale was firstly detected in metallic nanoresonators[42−47], due to the easier fabrication technology and more established characterization of these structures. The excitation of localized surface plasmon resonances (LSPRs) in metallic nanoparticles provides a strong field enhancement close to the metal surface, where the centrosymmetry of the material is broken and both third- and second-order nonlinear phenomena can be revealed. It took almost ten years before the first demonstration of harmonic generation in silicon nanodisks[48,49], but these pioneering studies immediately revealed two main advantages of dielectric over metallic nanostructures: negligible ohmic losses, and a remarkable field enhancement inside the resonator volume, which enables to exploit not only surface nonlinearity but also the stronger bulk nonlinearity in the whole volume. In dielectrics, Mie-type resonances originate when the diameter d of the nanoparticle is reduced so as to become comparable with the effective wavelength λ/n in the medium. At variance with their plasmonic counterparts, the first mode to appear (when $d \approx \lambda/n$) is a magnetic dipole resonance, and in turn the electromagnetic field can be concentrated in the core of the nanoparticles even for small sizes.

In this framework, the nanofabrication processes of III-V semiconductors guided-wave optics enabled the development of optical nanoantennas with non-centrosymmetric crystal structure and thus second-order nonlinear response. The most widely used materials are reported in Table 1, which provides a few factors that can explain the pros and cons of a given platform with respect to the others: 1) a high-refractive index n or, more precisely, the possibility to achieve a high refractive-index contrast between the nanoresonator and its substrate[①], which in turn determines how tightly the field can be confined; 2) a strong quadratic bulk susceptibility $\chi^{(2)} = 2d_{\mathrm{eff}}$; and 3) a broad transparency spectral window. These points motivated a series of experimental investigations on SHG in GaAs[50], $\mathrm{Al}_{0.18}\mathrm{Ga}_{0.82}\mathrm{As}$[51,52] and GaP[53] nanoresonators, with a maximum conversion efficiency $\eta_{\mathrm{SHG}} \approx 10^{-6}\ \mathrm{W}^{-1}$ [51,52], and more recently on

Table 1 | Most common materials for $\chi^{(2)}$ nonlinear nano-optics. Refractive index n and second-order nonlinear coefficient d all refer to a wavelength λ = 1550 nm but for LiNbO₃ for which we consider λ = 1313 nm.

Material	Point group	n	d_{eff} (pm/V)	λ_{TPA} (nm)	Refs.
GaAs	$\bar{4}3m$	3.38	110	1720	ref.[58,59]
$\mathrm{Al}_{0.18}\mathrm{Ga}_{0.82}\mathrm{As}$	$\bar{4}3m$	3.30	100	1480	ref.[60,61]
GaP	$\bar{4}3m$	3.10	82	1100	ref.[59]
AlN	$6mm$	2.10	4.7	440	ref.[62]
LiNbO₃	$3m$	2.30, 2.21	19.5	620	ref.[59]

---

① Among the refractive indices of monolithic or wafer-bonded substrates, let us recall that $n(\mathrm{SiO_2})$=1.45, $n(\mathrm{AlO}x)$=1.6, $n(\mathrm{Sapphire})$=1.75.

lithium niobate[54,55] and multi-quantum-well structures[56]. Currently, transition metal dichalcogenide[57] (TMDC) platforms are also being explored, but their performances are presently limited by fabrication technology and a smaller nonlinear overlap provided by these $\chi^{(2)}$ monolayers than nanoresonators, as it will be more clearly shown in the following.

Far from being a mere outcome of technological development, the micro-to-nano transition subtends a real paradigm change for optics, with analogies and striking differences between these two worlds. At variance with microcavities[63,64], nanoantennas are open systems with non-negligible coupling to free radiation[65], and the related nonlinear processes can be described as follows, within the formalism of non-Hermitian physics[66,67] (see Fig. 1):
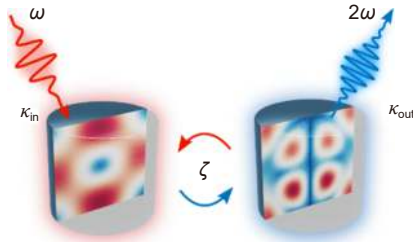

Fig. 1 | Simplified scheme of SHG in a leaky cavity. FF (SH) beam is represented in red (blue), κ_{in} (κ_{out}) denotes the input (output) coupling coefficient and ζ the spatial overlap between the dominant modes at the two frequencies.

- An external pump at fundamental frequency (FF) ω transfers a part of its energy to the resonator, by exciting its leaky eigenmodes with complex eigenfrequencies $\omega_m = \Omega_m - i\Gamma_m/2$;
- The coupling coefficient κ_{in}, which describes the injection efficiency into such modes, depends on their spectral and spatial overlap with the FF field;
- The eigenmode at FF couples with higher-order modes at the second harmonic (SH) through the quadratic susceptibility $\chi^{(2)}$. The coupling efficiency depends on the spatial overlap ζ of these modes, mediated by the nonlinear tensor;
- The field at 2ω is radiated with a time constant τ_m, which is inversely proportional to the mode quality factor $Q_m = \Omega_m/\Gamma_m$; the coupling efficiency with the different radiative channels are described by the coefficient κ_{out}.

Assuming for sake of simplicity that only two modes are involved, which we label with m at FF and l at SH respectively, we can quantify the SHG efficiency $\eta_{SHG} = P_{SH}/P_{FF}^2$ as[67,68]

$$\eta_{SHG} = |(\kappa_{in}Q_m)^2 \zeta_{lmm}\kappa_{out}Q_l|, \qquad (1)$$

where, with respect to the formulations in ref.[67,68], we included the spectral overlap inside the coupling coefficient. The mode spatial overlap ζ_{lmm} in (1) determines the selection rules for nonlinear generation in nanoresonators, which can be derived analytically for the particular case of a spherical resonator in a uniform medium[69], but generally have be computed numerically[67]. In the configuration of Fig. 1, the nanoresonator behaves like an antenna: it receives an external excitation, it stores the energy in the near field converting the FF signal to a localized current distribution at SH, and the latter radiates to the far field. In order to operate properly, an antenna has to maximize the radiated energy and the spectral bandwidth (low Q-factor), as well as the coupling with free space, i.e. impedance matching (high κ_{in}). Indeed, the first experimental investigations in this domain exploited low-order Mie-type resonances in dielectric nanoparticles, in many cases a magnetic dipole[48,52,70], with low quality factors (of the order of 10) as for most dipolar antennas[71]. These features are clearly different from those of guided optics: nanoantennas operate in free space and can be integrated in optical cavities; they can provide a larger in- and out-coupling efficiency than the evanescent coupling adopted in many guided systems, and they typically exhibit a broader spectral and spatial acceptance.

However, as it is clear from Eq. (1), maximizing SHG requires high-Q resonances. Ideally, one would envisage suppressing all the radiation channels apart from those used to inject and extract power, in order to both efficiently pump the resonator and increase the quality factor of the nonlinearly interacting modes. In recent years, several strategies have been proposed for boosting nonlinear generation by optimizing optical confinement[72,73], through anapole states[53,74–77] or high-Q BIC modes[68,78,79], and controlling SH radiation pattern[80–85] or polarization properties[52,86,87].

These theoretical and experimental studies allowed to extensively investigate nonlinear optical effects in open cavities and engineer their emission properties. However, for many practical purposes, it is clearly more advantageous to dispose of these elementary units, called in the following meta-atoms, in large arrays. According to the specific end, different solutions have been explored and they will be analyzed in detail in the next section.

To provide a fair comparison in terms of frequency-conversion performances, a unique figure of merit has to be defined. Hereafter, we will refer to the power-independent conversion efficiency $\eta_{\mathrm{SHG}} = P_{\mathrm{SH}}/P_{\mathrm{FF}}^2 \, (\mathrm{W}^{-1})$. However, in some cases, the conversion ratio $\beta_{\mathrm{SHG}} = P_{\mathrm{SH}}/P_{\mathrm{FF}}$ will be reported along with the peak pump power P_{FF}, to provide a helpful indication of the maximum SHG power before the onset of saturation or other undesired effects. All the reported powers refer to peak values of temporal pulses.

SHG in all-dielectric metasurfaces

Arranging nanoantennas in 2D arrays, i.e. metasurfaces, not only increases the active surface and in turn the non-linearly generated power, but it also enables a mutual interaction among the meta-atoms as an additional degree of freedom to control nonlinear emission. The field perceived by each nanoantenna in the array is the sum of the incident and the scattered waves by all the neighboring elements. According to the ratio of these two contributions, one of the two following regimes prevails:

• **Far-field interaction.** For large inter-particle distances, but still in the sub-diffraction limit, mutual interactions act as a minor perturbation. The effect of the scattered field by the nanoparticles in the array is to slightly enhance the electromagnetic field confinement and the quality factor of the resonant modes, yet the main radiation properties of isolated meta-atoms stay unaltered.

• **Near-field interaction.** In compact arrays, optical coupling between close neighbors can strongly perturb the resonant behavior of isolated nanoparticles and promote the onset of high-Q delocalized modes, which are particularly interesting for nonlinear generation.

It is also worth mentioning that for larger periods, comparable with the incident wavelength, the in-plane first diffraction order is no longer evanescent (Rayleigh anomaly) and additional peaks, due to surface lattice resonances, appear in the extinction spectrum[88,89]. This case will not be analyzed in detail in the present work, and we therefore refer the interested reader to thematic reviews[90−92].

Let us also remark in passing that optical nanocavities and metasurfaces have been often suggested as an intriguing solution to avoid the well-known need of phase matching in microcavities. However, it is worth noting that such statement is not entirely appropriate for two reasons: 1) since phase matching is a condition aimed at maximizing the in-phase oscillation of overlapped FF

and SH fields, it is not a problem to avoid but an opportunity to exploit; 2) its concept stems from the overlap integral ζ_{lmm} which, in translationally or rotationally invariant cavities, can be decomposed in a transverse and a propagative contribution. In nanocavities this decomposition is no longer feasible, but still ζ_{lmm} has an amplitude and phase which has to be taken into account to maximize SHG efficiency[67], especially in the case of delocalized collective resonances.

Quasi-independent nanoantennas

In the radio-frequency (RF) domain, antenna arrays are used to control the far-field properties of emitted signals. In that case, local sources enable to separately drive each element of the array whose behavior is totally independent. In the case of metasurfaces for nonlinear optics the scenario is a bit different. The driving term usually stems from free radiation and non-Hermitian cavities are always coupled due to their leaky nature, even if their distance is large compared to the wavelength[93]. This especially holds true for low-order Mie resonances like electric (ED) and magnetic (MD) dipoles, insofar as they strongly scatter light in the far field. However, for arrays of Si nanoparticles with a period large enough to apply coupled-dipole approximation, it was shown that the scattering properties at wavelengths larger than the inter-particle distance are mostly determined by the scattering properties of individual constituents[89]. Figure 2(a) compares the near-IR scattering spectrum of an isolated GaAs nanocylinder, computed with perfectly matched layers at the borders of the simulation domain, and the transmission spectrum of arrayed elements with sub-λ distance. Decomposing the field inside a nanocylinder of the array into vector spherical wavefunctions, it appears that the dips in the transmission spectrum of the array originate from Mie-type resonances of isolated elements, rather than non-local Bragg resonances typical of the photonic crystal regime[94]. The in-plane scattering of neighboring structures essentially results in an electromagnetic-field enhancement inside the nanoparticle volume, see Fig. 2(b), and a partial blue-shift of Mie-type resonances at large wavelengths, whereas additional lattice resonances appear when the wavelength is comparable with the period.

These features were formerly exploited to enhance the nonlinear generation from nanocylinders relying on the properties of isolated elements, for the design of metasurfaces working in the sub-λ regime at FF and featuring
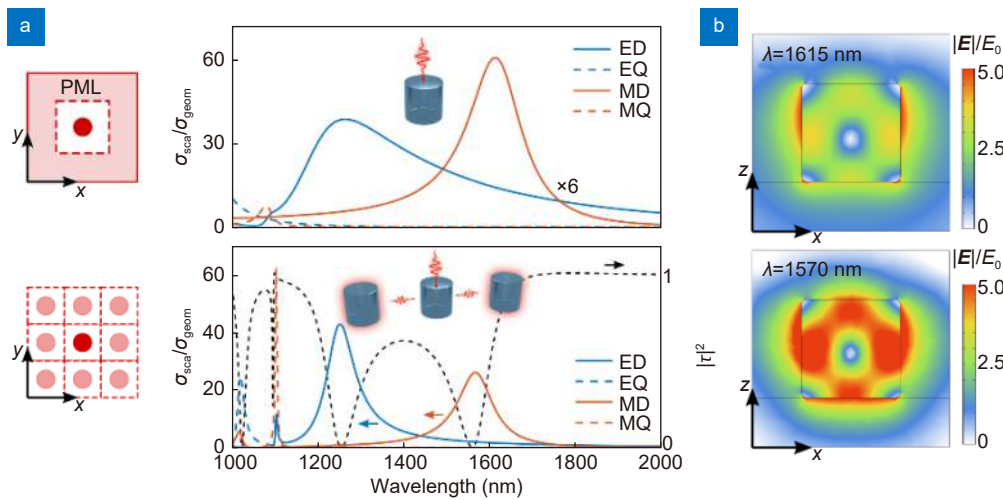
Fig. 2 | Comparison between isolated (top) and arrayed (bottom) air-suspended GaAs nanoantennas with radius *r* = 200 nm and height *h*=400 nm. A normally impinging beam is linearly polarized along *x*, and the array (bottom) has a period of *p*=1 μm. (**a**) Scattering cross section decomposed in electric (blue) and magnetic (red) multipolar contributions, computed by projecting the field inside a nanoparticle onto vector spherical harmonics[95]. The scattering cross section from the isolated particle has been scaled by a factor 6 to be compared with the plot on the bottom. The black dashed curve (bottom) displays the array transmission. (**b**) Near-field enhancement corresponding to the magnetic-dipole resonance.
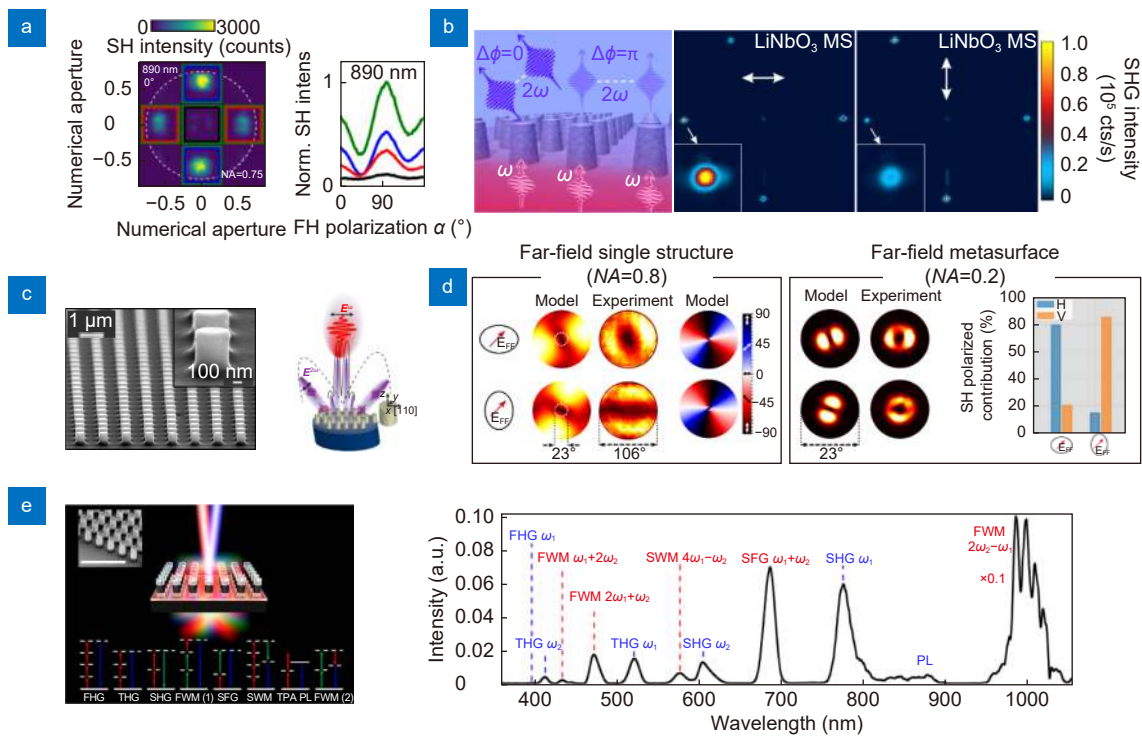

Fig. 3 | Arrays of quasi-independent dielectric χ⁽²⁾ Mie-type resonators. (**a**) SHG from a GaAs metasurface radiated into different diffraction orders vs. pump polarization angle. Green: total; blue: (0,±1) orders; red: (±1,0) orders; black: (0,0) order[98]. (**b**) SH back-focal plane (BFP) imaging of a LiNbO₃ metasurface for horizontally (center) or vertically (right) polarized pump[101]. (**c**) Mechanism to partially redirect SHG from an AlGaAs metasurface close to normal direction[99]. (**d**) Controlling SH polarization. BFP imaging of SH from isolated (left) or arrayed (right) AlGaAs nanoantennas with elliptical basis[100]. (**e**) Broadband frequency generation in a GaAs metasurface through multiple nonlinear processes[96].

diffraction lobes at harmonic frequencies[48,50,54,96–102]. Some representative examples are shown in Fig. 3, but more in general this approach was adopted for SHG in the near-IR[54,99,100], visible[50,98,101] and ultraviolet[97] windows,

as well as to control its polarization and diffraction properties[98–101] or design frequency mixers[96]. In most of the cases, a magnetic dipole resonance is employed at FF, as this is the first mode appearing at large wavelengths in

dielectrics[25], which both enhances the field inside the resonator volume and keeps its size small. The choice of the period is usually aimed at maximizing the density of resonators in the array, while keeping the role of non-local interactions weak.

Within this approach, in analogy with antennas arrays in the RF domain, the total SH far-field intensity $I_{\text{tot}}^{\text{far}}$ emitted from the metasurface can be written as the sum of N quasi-independent emitters:

$$I_{\text{tot}}^{\text{far}}(\theta, \phi) = |A(\theta, \phi)|^2 I_0^{\text{far}}(\theta, \phi) \ ,$$

where $A(\theta, \phi)$ is the array factor and $I_0^{\text{far}}(\theta, \phi)$ is the emission from a single element. The role of the array is therefore to modulate the radiation pattern of the isolated emitter. While for a given metasurface $A(\theta, \phi)$ is set, one can modify the nonlinearly excited modes and $I_0^{\text{far}}(\theta, \phi)$ by changing the pump configuration (e.g. its polarization)[67,103]. In turn, depending on the state of the pump, the nonlinear emission can be funneled into different diffraction lobes, see Fig. 3(a, b). However, in many cases of practical interest it is more convenient to control the SH polarization while staying in the same diffraction order (e.g. the zero-diffraction order for on-axis applications). In these circumstances the lattice constant can be optimized to maximize the overlap between $|A(\theta, \phi)|^2$ and $I_0^{\text{far}}(\theta, \phi)$ and partially redirect the nonlinear generation, see Fig. 3(c, d).

The low-Q antenna regime lends also itself to nonlinear beam shaping applications, as it can combine a broad spectral bandwidth with a large coupling to free space. At

variance with linear metasurfaces, where resonances are usually detrimental for wavefront shaping[104], here a strong local field enhancement and thus resonances are necessary for an efficient nonlinear conversion, as highlighted in the previous section. In recent years, two main mechanisms have been shown to encode the harmonic field phase: 1) tuning of the interaction between FF and SH modes by changing the size of the meta-atoms; 2) extension of Pancharatnam-Berry phase concept to the nonlinear regime[105].

The former was inspired by a series of works on ultrathin plasmonic metasurfaces[110,111] and later extended to third harmonic generation[112,113]. More recently, it was investigated in detail to design highly directional emitters implementing the first Kerker condition at harmonic frequencies, and thus to reproduce the concept of Huygens' metasurfaces in the nonlinear regime. Wang et al.[106] predicted that balancing the excitation of modes with opposite symmetry is possible to extract a set of resonators with unidirectional THG covering the whole $[0, 2\pi]$ phase range. They experimentally validated this approach with a Si metasurface steering the THG beam into the first diffraction order, with a record 92% efficiency, see Fig. 4(a). The possibility to upconvert an optical signal and control its wavefront within a sub-micrometer-thick metasurface is not only attractive for scalability and integrability purposes, but it also enables to manufacture optical devices that would not be otherwise conceivable with bulk elements. This idea allowed e.g. to study the spatial correlation between an object and its upconverted
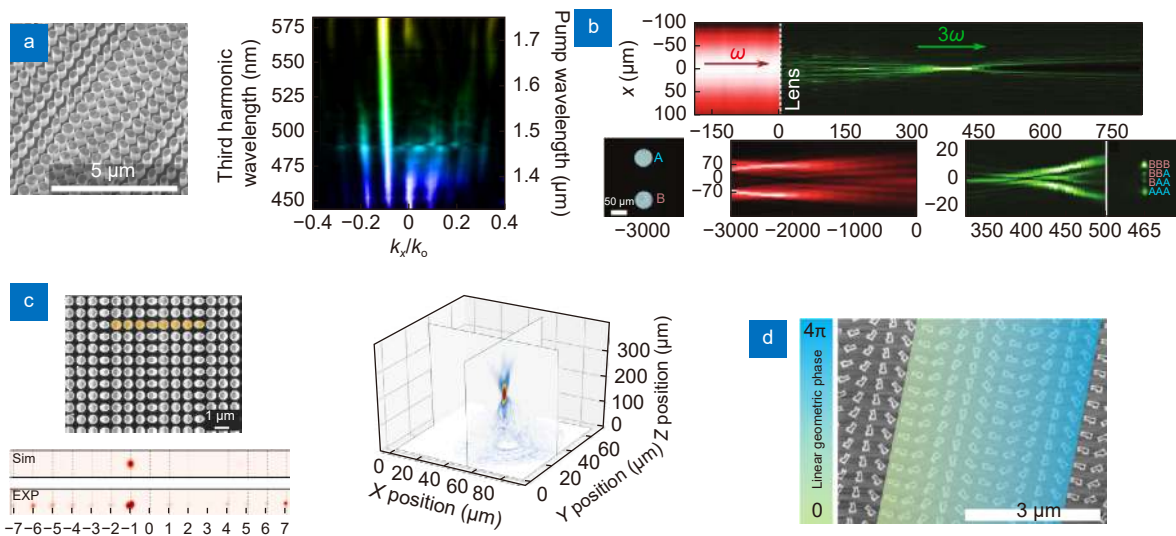
Fig. 4 | Nonlinear wavefront shaping in dielectric metasurfaces. (**a**) Si metasurface implementing the first Kerker condition and funneling THG into the (-1)-diffraction order[106]. (**b**) Top: TH focusing from a Si metasurface. Bottom: Nonlinear imaging and spatial correlation for two apertures[107]. (**c**) SH beam-steering (left) and focusing (right) from an AlGaAs metasurface[108]. (**d**) SH geometric phase control in a Si metasurface[109].

image, when observed through a nonlinear meta-lens, and generalize the lens equation to the nonlinear regime[107,114], see Fig. 4(b).

The extension of this first resonant approach to the SH case was not straightforward due to the selection rules imposed by the $\chi^{(2)}$ tensor of most widely used non-centrosymmetric materials, which lead to a null on-axis SHG from axially symmetric nanoparticles, impractical for many applications. A workaround solution to this issue was recently demonstrated thanks to AlGaAs-on-sapphire meta-atoms, with a broken symmetry that helps to rephase the two SH radiation lobes at large angles and favors normal emission[108]. Such concept was validated on SH beam steering and focusing, see Fig. 4(c), with a normalized conversion efficiency $\eta_{SHG} \sim 2.8 \times 10^{-10} \, W^{-1}$.

On the other hand, nonlinear geometric-phase control in centrosymmetric metasurfaces relies on the following idea: when a nanostructure with m-fold rotational symmetry is excited by a pump beam with circular polarization state σ, the n-th harmonic dipole moment acquires a phase $e^{(n\pm 1)i\sigma\theta}$, where θ is the rotation angle of the nanostructure and the '+' and '–' signs correspond to the same and opposite circular polarization with respect to the pump beam, respectively[105]. The symmetry order m imposes selection rules on harmonic generation as only the orders $n = lm\pm 1$, with l an integer, are allowed. This principle was validated by a series of explorations on C2 and C3 symmetric metallic nanostructures for THG and SHG, respectively[105,114–116]. More recently, the same mechanism was exploited to encode the phase in Si nano-blocks and demonstrate TH holography in all-dielectric metasurfaces with a factor-40 generation enhancement with respect to a bare Si film[117]. Bar-David et al.[109] also showed that centrosymmetry breaking close to the surfaces can be exploited in Si, as done in plasmonic nanoparticles, to induce an effective second-order nonlinearity. Resorting to C1-symmetric meta-atoms, see Fig. 4(d), it was therefore possible to manipulate SH phase in dielectric metasurfaces, yet with a generation efficiency 4 orders of magnitude lower than in metals, which can be attributed to a much smaller field enhancement at the surfaces compared to the case of LSPR. Compared to the previous approach, geometric phase control offers unique advantages as it directly ensures an equal emission amplitude from the different meta-atoms and it requires the optimization of a single structure.

The above-mentioned shaping techniques rely solely on the geometry of the resonators. A different solution, recently demonstrated by Dasgupta et al.[118], relies on the strong spin-orbit coupling, due to degenerate valleys in TMDC monolayers, to generate optical vortex at the SH with different topological charges. The valley-dependent spin selection rules, in combination with Mie-resonances, might offer a further degree of control on the properties of the generated beam in analogue way as reported for hybrid Au-WS$_2$ metasurfaces[119].

Collective resonances in nonlinear metasurfaces

Mie resonators are highly multi-mode open cavities. Their eigenmodes, being non strictly orthogonal within the resonator volume[120], can either interfere giving rise to Fano resonances[13,15] or strongly couple to each other, originating Friedrich-Wintgen BICs[21,22]. Exploiting this approach, Koshelev et al.[68] reported an experimental record quality factor $Q \sim 188$ in an isolated AlGaAs resonator with a maximum SHG efficiency $1.3 \times 10^{-6} \, W^{-1}$. To go beyond this value, one can either increase the resonator size to excite high-Q whispering gallery modes as in micro-disks or exploit interference between multiple nanoantennas. The latter option was first demonstrated by Yang et al.[121] to boost THG in Si metasurfaces. The coupling between a bright and broad ED mode and a dark MD with smaller damping results in a sharp Fano resonance with an experimental $Q \sim 466$ in the transmittance spectrum. The same structure was exploited to enhance high harmonic generation[122] and design lithium niobate metasurfaces for SHG[123]. In the latter case, a sharp Fano resonance ($Q \sim 2350$) was theoretically predicted to enhance SH conversion up to a value $\beta_{SHG} \sim 3.2 \times 10^{-4}$ for a pump intensity $I_{FF} = 3.2$ GM/cm².

The symmetry of modes in periodic structures plays a central role to confine photons for longer times and thereby boost nonlinear generation. As was shown for photonic-crystal slabs[128] or lamellar gratings[129], the presence of guided resonances or asymmetric Bloch modes, which are symmetry protected at normal incidence, can result in sharp peaks in the transmission spectrum with a typical Fano line shape, as soon as the in-plane $\boldsymbol{k}$-vector is different from zero. When the symmetry of the system is perfectly preserved, i.e. in the case of a normally impinging plane wave on a symmetric array, modes with opposite symmetry are completely decoupled promoting the creation of BIC modes infinitely confined in the structure[130] ($Q \to \infty$). Please note that, strictly speaking, symmetry protected BIC modes exist only in infinite

structures, and the presence of an edge would destroy this condition. By reciprocity, these modes cannot be excited from free space and they are not of practical interest. However, by slightly breaking the symmetry of the system, one can observe the presence of quasi-BIC modes with large quality factors. This result can be achieved either by slightly tilting the incident beam or by carefully designing asymmetric meta-atoms. Several configurations are analyzed and compared in ref.[131], and they have been the initial guess for the design of many nonlinear metasurfaces, see Fig. 5. Relying on the broken symmetry resonators proposed in ref.[132], Vabishchevich et al. demonstrated a GaAs metasurface with a maximum field intensity enhancement $|E|^2/E_0^2 \sim 500$ inside the resonators volume and $Q \sim 500$, see Fig. 5(a), resulting in three-times higher SHG conversion efficiency than in nanodisk metasurfaces with a standard MD resonance[50]. In the Fano picture, such symmetry breaking can be seen as the introduction of a coupling term between bright and broad resonances with dark and narrow ones, which would be otherwise uncoupled by symmetry. The close link between quasi-BIC modes and the appearance of Fano resonances was adopted to design several meta-atoms with broken symmetry to enhance nonlinear effects. In ref.[133], the authors resort to spindle-shaped Si nanoparticles to implement a metasurface that features a resonance with $Q = 1.6 \times 10^5$ and 300 times enhanced THG with respect to a uniform slab. Similarly, ref. [125] reports a maximum TH conversion ratio $\beta_{THG} = P_{TH}/P_{FF} \sim 3.2 \times 10^{-4}$ for $P_{FF} \sim 8.1$ kW relying

on meta-atoms made of two Si nanorods with different sizes, see Fig. 5(b). Importantly, in the same work the authors demonstrate the central role played by the nonradiative losses due to surface roughness, structural disorder and finite size of the array. The total quality factor Q exhibits a radiative (Q_r) and a non-radiative (Q_{nr}) contribution according to $1/Q = 1/Q_{nr} + 1/Q_r$, and the maximum conversion efficiency is achieved at critical coupling ($Q_r = Q_{nr}$).

The same meta-atoms have also been used to boost the nonlinear response of TMD monolayers. In ref.[66] the authors measured a SHG enhancement of ≈ 1140 times with respect to the bulk Si film, in a layer of tungsten disulfide (WS_2) deposited on a Si metasurface exhibiting a quasi-BIC with $Q = 35$ at critical coupling. A collective resonance with Q-factor ≈ 550 from a similar Si metasurface was also exploited in ref.[134] to boost the nonlinearity of an MoS_2 monolayer, detecting a maximum conversion efficiency $\eta_{SHG} \sim 5.2 \times 10^{-12}$ W^{-1}.

A larger non-radiative $Q \approx 1.8 \times 10^4$ was experimentally achieved with Si nanoblocks[126] featuring a symmetry breaking along one in-plane direction, see Fig. 5(c). However, due to their available broadband short-pulse source, the authors could only obtain a conversion efficiency $\eta_{SHG} \sim 3.6 \times 10^{-11}$ W^{-1} exploiting a resonance with a smaller $Q \approx 4 \times 10^3$.

The last symmetry breaking mechanism shown in Fig. 5(d) relies on zigzag arrays of nanocylinders with elliptical basis. The high-Q resonance due to the quasi-BIC mode and the strong field enhancement close to the res-
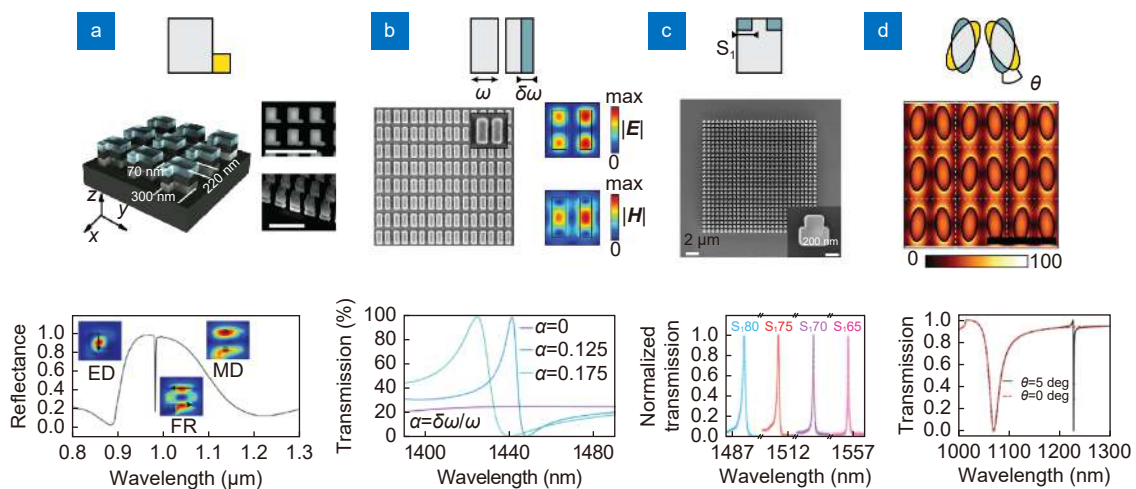
Fig. 5 | Quasi-BIC mode generation in nonlinear metasurfaces. A few ways to break the symmetry and reveal the high-Q resonance are sketched in the top row. Yellow (blue) color denotes a material addition (removal). (**a**) L-shaped GaAs/AlGaO heterostructures[124]. (**b**) Asymmetric Si nanodimers made of two rods with different widths[125]. (**c**) T-shaped Si resonators[126]. (**d**) Asymmetric GaP nanodimers made of two elliptical-basis cylinders rotated by an angle θ[127].

onators surface proved exquisite ingredients to improve metasurface-based biosensing[26,28]. By adopting this approach, Anthur et al.[127] demonstrated a GaP metasurface featuring a high-Q resonance ($\sim 2 \times 10^3$) and a SHG efficiency $\eta_{SHG} \sim 5.4 \times 10^{-7}$ W^{-1} in continuous-wave regime, which constitutes one of the most promising result in the near-IR with metasurfaces to date.

Conclusion and outlook

Most of the aforementioned studies aimed at optimizing the electromagnetic field confinement inside the metasurfaces, with the primary goal of enhancing nonlinear conversion efficiency. Let us therefore compare their performances with those of other more established photonic platforms aiming at the same target through different physical phenomena.

Figure 6 reports the SHG efficiencies of several published works in the last two decades, grouped according to different types of devices and materials. Guided systems like optical waveguides[62,135], ring[136–138] or disk[139–144] resonators provide tight electromagnetic field confinement in nonlinear materials for long propagation distances, leading in turn to huge conversion efficiencies (up to 10^3 W^{-1}). However, the disks featuring the best performances have a large footprint (of the order of the mm^2 i.e. not fully compatible with high integration), while conversion efficiencies drop to $10^{-4} - 10^{-2}$ W^{-1} for smaller LiNbO$_3$ and GaAs microdisks.
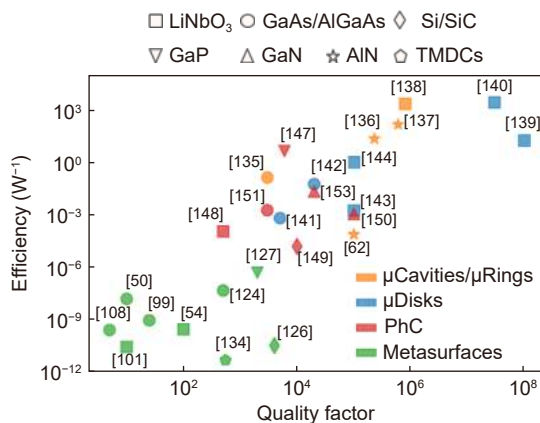

Fig. 6 | SHG efficiency vs. Q-factor of the dominant FF mode for different resonant devices (markers' color) and materials (markers' shape).

Phased-matched guided systems enable high generation efficiency, but they are typically not well suited when a large coupling with free radiation is required or when light confinement has to be squeezed to nanometric volumes. In this perspective, photonic-crystal waveguides[145] and nanocavities[146] gained an increasing interest in the community. The creation of defect states in photonic-crystal slabs (e.g. L3 cavities) enabled to confine the normally impinging light in ultra-small mode volumes and enhance SHG in III-V devices[147–151].

However, in photonic crystals as well as in metasurfaces, a maximized generation efficiency stems from a well-balanced compromise between field enhancement and mode volume. Indeed, the exploitation of spatially extended resonances can increase the effective interaction volume between harmonic fields and boost nonlinear conversion. Based on the concept of symmetry-protected BIC introduced in Section *SHG in all-dielectric metasurfaces*, Minkov et al.[152] designed a doubly resonant photonic crystal slab heterostructure providing a fully confined defect mode inside the photonic bandgap at FF and a resonant quasi-BIC mode inside the light cone at SH. Wang et al.[153] experimentally demonstrated that, when pumped at normal direction, such structure generates a radially polarized SH with a conversion efficiency $\eta_{SHG} = 2.4 \times 10^{-2}$ W^{-1}. This good performance arises from the fulfillment of a doubly resonant condition and the optimization of the nonlinear overlap integral ζ_{lmm}[152].

The comparison reported in Fig. 6 brings us to a first relevant conclusion: if one considers conversion efficiency as the sole target, to date guided systems provide the best performances by orders of magnitude over all other platforms. On the other hand, both photonic crystals and metasurfaces offer unprecedented opportunities for integrability[154], on-axis applications[153], ultra-fast switching[35,37,155], and emission control[156]. Metasurfaces appear inherently more robust to the breaking of translational invariance induced by the presence of the edges, and as such more effective to achieve strong resonant enhancement also for small footprints[126].

In conclusion, we have reviewed the recent progress in the rapidly evolving domain of all-dielectric $\chi^{(2)}$ metasurfaces. At least two possible outlooks emerged for these devices.

On one side, resorting to coupled nanoantennas and collective resonances seems the wisest strategy to maximize nonlinear generation. However, also the metasurfaces exhibiting the largest quality factors are orders of magnitude less efficient than the other platforms in Fig. 6. This outcome stems from the fact that to date most of the studies adopting this approach, and discussed in

Section *SHG in all-dielectric metasurfaces*, focused on the creation of a single high-Q resonance around FF. Instead, we expect that such gap with the other technologies may be filled with a careful design providing a good balance between free-space coupling and mode quality factors, while implementing a doubly resonant condition and optimizing the nonlinear overlap integral, as described in Eq. (1).

On the other side, low-Q antennas represent a true change of paradigm with respect to both guided structures and photonic crystals. Their presently lower SHG efficiency is largely counterbalanced by intriguing possibilities ranging from the dynamic tunability of individual meta-atom emission[82,155,157,158], pulse shaping[159], broadband parametric devices[96], nonlinear imaging[107], wavefront shaping[108] and meta-holography[112,160,161]. Their rapid development is currently underpinned by an ongoing progress in nanofabrication, new promising nonlinear materials like TMDCs, and both analytical[69,162] and numerical[67] methods to model nonlinear generation in leaky cavities. The improvement of such mathematical tools seems especially important for non-intuitive design and optimization of highly multi-mode nanoresonators[163].

Based on the impressive achievements of this new branch of nonlinear optics, we expect a new class of nonlinear photonic meta-devices to arise in the forthcoming years, for high-speed switching, entangled photon sources, supercontinuum generation and nonlinear imaging.

References

1. Koenderink AF, Alù A, Polman A. Nanophotonics: shrinking light-based technology. *Science* **348**, 516–521 (2015).
2. Novotny L, van Hulst N. Antennas for light. *Nat Photonics* **5**, 83–90 (2011).
3. Giannini V, Fernández-Domínguez AI, Heck SC, Maier SA. Plasmonic nanoantennas: fundamentals and their use in controlling the radiative properties of nanoemitters. *Chem Rev* **111**, 3888–3912 (2011).
4. Schuller JA, Barnard ES, Cai WS, Jun YC, White JS et al. Plasmonics for extreme light concentration and manipulation. *Nat Mater* **9**, 193–204 (2010).
5. Baumberg JJ, Aizpurua J, Mikkelsen MH, Smith DR. Extreme nanophotonics from ultrathin metallic gaps. *Nat Mater* **18**, 668–678 (2019).
6. Pelton M. Modified spontaneous emission in nanophotonic structures. *Nat Photonics* **9**, 427–435 (2015).
7. Anger P, Bharadwaj P, Novotny L. Enhancement and quenching of single-molecule fluorescence. *Phys Rev Lett* **96**, 113002 (2006).
8. Curto AG, Volpe G, Taminiau TH, Kreuzer MP, Quidant R et al. Unidirectional emission of a quantum dot coupled to a nanoantenna. *Science* **329**, 930–933 (2010).
9. Shaltout AM, Shalaev VM, Brongersma ML. Spatiotemporal light control with active metasurfaces. *Science* **364**, eaat3100 (2019).
10. Kamali SM, Arbabi E, Arbabi A, Faraon A. A review of dielectric optical metasurfaces for wavefront control. *Nanophotonics* **7**, 1041–1068 (2018).
11. Zhang Y B, Liu H, Cheng H, Tian J G, Chen S Q. Multidimensional manipulation of wave fields based on artificial microstructures. *Opto-Electron Adv* **3**, 200002 (2020).
12. Notomi M. Manipulating light with strongly modulated photonic crystals. *Rep Prog Phys* **73**, 096501 (2010).
13. Luk'yanchuk B, Zheludev NI, Maier SA, Halas NJ, Nordlander P et al. The Fano resonance in plasmonic nanostructures and metamaterials. *Nat Mater* **9**, 707–715 (2010).
14. Miroshnichenko AE, Flach S, Kivshar YS. Fano resonances in nanoscale structures. *Rev Mod Phys* **82**, 2257–2298 (2010).
15. Limonov MF, Rybin MV, Poddubny AN, Kivshar YS. Fano resonances in photonics. *Nat Photonics* **11**, 543–554 (2017).
16. Kerker M, Wang DS, Giles CL. Electromagnetic scattering by magnetic spheres. *J Opt Soc Am* **73**, 765–767 (1983).
17. Person S, Jain M, Lapin Z, Sáenz JJ, Wicks G et al. Demonstration of zero optical backscattering from single nanoparticles. *Nano Lett* **13**, 1806–1809 (2013).
18. Fu YH, Kuznetsov AI, Miroshnichenko AE, Yu YF, Luk'yanchuk B. Directional visible light scattering by silicon nanoparticles. *Nat Commun* **4**, 1527 (2013).
19. Miroshnichenko AE, Evlyukhin AB, Yu YF, Bakker RM, Chipouline A et al. Nonradiating anapole modes in dielectric nanoparticles. *Nat Commun* **6**, 8069 (2015).
20. Monticone F, Alù A. Embedded photonic eigenvalues in 3D nanostructures. *Phys Rev Lett* **112**, 213903 (2014).
21. Rybin MV, Koshelev KL, Sadrieva ZF, Samusev KB, Bogdanov AA et al. High-Q supercavity modes in subwavelength dielectric resonators. *Phys Rev Lett* **119**, 243901 (2017).
22. Bogdanov AA, Koshelev KL, Kapitanova PV, Rybin MV, Gladyshev SA et al. Bound states in the continuum and fano resonances in the strong mode coupling regime. *Adv Photonics* **1**, 016001 (2019).
23. Fang CZ, Yang QY, Yuan QC, Gan XT, Zhao JL et al. High-Q resonances governed by the quasi-bound states in the continuum in all-dielectric metasurfaces. *Opto-Electron Adv* **4**, 200030 (2021).
24. Khurgin JB. How to deal with the loss in plasmonics and metamaterials. *Nat Nanotechnol* **10**, 2–6 (2015).
25. Kuznetsov AI, Miroshnichenko AE, Brongersma ML, Kivshar YS, Luk'yanchuk B. Optically resonant dielectric nanostructures. *Science* **354**, aag2472 (2016).
26. Tittl A, Leitis A, Liu MK, Yesilkoy F, Choi DY et al. Imaging-based molecular barcoding with pixelated dielectric metasurfaces. *Science* **360**, 1105–1109 (2018).
27. Yavas O, Svedendahl M, Dobosz P, Sanz V, Quidant R. On-a-chip biosensing based on all-dielectric nanoresonators. *Nano Lett* **17**, 4421–4426 (2017).
28. Yesilkoy F, Arvelo ER, Jahani Y, Liu MK, Tittl A et al. Ultrasensitive hyperspectral imaging and biodetection enabled by dielectric metasurfaces. *Nat Photonics* **13**, 390–396 (2019).
29. Bozhevolnyi SI, Khurgin JB. The case for quantum plasmonics. *Nat Photonics* **11**, 398–400 (2017).

30. Stav T, Faerman A, Maguid E, Oren D, Kleiner V et al. Quantum entanglement of the spin and orbital angular momentum of photons using metamaterials. *Science* **361**, 1101–1104 (2018).

31. Liu J, Shi MQ, Chen Z, Wang SM, Wang ZL et al. Quantum photonics based on metasurfaces. *Opto-Electron Adv* **4**, 200092 (2021).

32. Smirnova D, Kivshar YS. Multipolar nonlinear nanophotonics. *Optica* **3**, 1241–1255 (2016).

33. Caspani L, Xiong CL, Eggleton BJ, Bajoni D, Liscidini M et al. Integrated sources of photon quantum states based on nonlinear optics. *Light Sci Appl* **6**, e17100 (2017).

34. Marty G, Combrié S, Raineri F, De Rossi A. Photonic crystal optical parametric oscillator. *Nat Photonics* **15**, 53–58 (2021).

35. Husko C, De Rossi A, Combrié S, Tran QV, Raineri F et al. Ultrafast all-optical modulation in GaAs photonic crystal cavities. *Appl Phys Lett* **94**, 021111 (2009).

36. Koos C, Vorreau P, Vallaitis T, Dumon P, Bogaerts W et al. All-optical high-speed signal processing with silicon-organic hybrid slot waveguides. *Nat Photonics* **3**, 216–219 (2009).

37. Nozaki K, Tanabe T, Shinya A, Matsuo S, Sato T et al. Sub-femtojoule all-optical switching using a photonic-crystal nanocavity. *Nat Photonics* **4**, 477–483 (2010).

38. Krasnok A, Tymchenko M, Alù A. Nonlinear metasurfaces: a paradigm shift in nonlinear optics. *Mater Today* **21**, 8–21 (2018).

39. Pertsch T, Kivshar Y. Nonlinear optics with resonant metasurfaces. *MRS Bull* **45**, 210–220 (2020).

40. Sain B, Meier C, Zentgraf T. Nonlinear optics in all-dielectric nanoantennas and metasurfaces: a review. *Adv Photonics* **1**, 024002 (2019).

41. Li GX, Zhang S, Zentgraf T. Nonlinear photonic metasurfaces. *Nat Rev Mater* **2**, 17010 (2017).

42. Lippitz M, van Dijk MA, Orrit M. Third-harmonic generation from single gold nanoparticles. *Nano Lett* **5**, 799–802 (2005).

43. Danckwerts M, Novotny L. Optical frequency mixing at coupled gold nanoparticles. *Phys Rev Lett* **98**, 026104 (2007).

44. Hanke T, Krauss G, Träutlein D, Wild B, Bratschitsch R et al. Efficient nonlinear light emission of single gold optical antennas driven by few-cycle near-infrared pulses. *Phys Rev Lett* **103**, 257404 (2009).

45. Baida H, Mongin D, Christofilos D, Bachelier G, Crut A et al. Ultrafast nonlinear optical response of a single gold nanorod near its surface plasmon resonance. *Phys Rev Lett* **107**, 057402 (2011).

46. Biagioni P, Brida D, Huang JS, Kern J, Duò L et al. Dynamics of four-photon photoluminescence in gold nanoantennas. *Nano Lett* **12**, 2941–2947 (2012).

47. Celebrano M, Wu XF, Baselli M, Großmann S, Biagioni P et al. Mode matching in multiresonant plasmonic nanoantennas for enhanced second harmonic generation. *Nat Nanotechnol* **10**, 412–417 (2015).

48. Shcherbakov MR, Neshev DN, Hopkins B, Shorokhov AS, Staude I et al. Enhanced third-harmonic generation in silicon nanoparticles driven by magnetic response. *Nano Lett* **14**, 6488–6492 (2014).

49. Shcherbakov MR, Shorokhov AS, Neshev DN, Hopkins B, Staude I et al. Nonlinear interference and tailorable third-harmonic generation from dielectric oligomers. *ACS Photonics* **2**, 578–582 (2015).

50. Liu S, Sinclair MB, Saravi S, Keeler GA, Yang YM et al Resonantly enhanced second-harmonic generation using III-V semiconductor all-dielectric metasurfaces. *Nano Lett* **16**, 5426–5432 (2016);
http://doi.org/10.1021/acs.nanoLett.6b01816.

51. Gili VF, Carletti L, Locatelli A, Rocco D, Finazzi M et al. Monolithic AlGaAs second-harmonic nanoantennas. *Opt Express* **24**, 15965–15971 (2016).

52. Camacho-Morales R, Rahmani M, Kruk S, Wang L, Xu L et al. Nonlinear generation of vector beams from AlGaAs nanoantennas. *Nano Lett* **16**, 7191–7197 (2016).

53. Grinblat G, Li Y, Nielsen MP, Oulton RF, Maier SA. Enhanced third harmonic generation in single germanium nanodisks excited at the anapole mode. *Nano Lett* **16**, 4635–4640 (2016).

54. Fedotova A, Younesi M, Sautter J, Vaskin A, Löchner FJF et al. Second-harmonic generation in resonant nonlinear metasurfaces based on lithium niobate. *Nano Lett* **20**, 8608–8614 (2020).

55. Timpu F, Sendra J, Renaut C, Lang L, Timofeeva M et al. Lithium niobate nanocubes as linear and nonlinear ultraviolet mie resonators. *ACS Photonics* **6**, 545–552 (2019).

56. Shen KC, Huang YT, Chung TL, Tseng ML, Tsai WY et al. Giant efficiency of visible second-harmonic light by an all-dielectric multiple-quantum-well metasurface. *Phys Rev Appl* **12**, 064056 (2019).

57. Busschaert S, Reimann R, Cavigelli M, Khelifa R, Jain A et al. Transition metal dichalcogenide resonators for second harmonic signal enhancement. *ACS Photonics* **7**, 2482–2488 (2020).

58. Adachi S. Optical dispersion relations for GaP, GaAs, GaSb, InP, InAs, InSb, $Al_xGa_{1-x}As$, and $In_{1-x}Ga_xAs_yP_{1-y}$. *J Appl Phys* **66**, 6030–6040 (1989).

59. Shoji I, Kondo T, Kitamoto A, Shirane M, Ito R. Absolute scale of second-order nonlinear-optical coefficients. *J Opt Soc Am B* **14**, 2268–2294 (1997).

60. Gehrsitz S, Reinhart FK, Gourgon C, Herres N, Vonlanthen A et al. The refractive index of $Al_xGa_{1-x}As$ below the band gap: accurate determination and empirical modeling. *J Appl Phys* **87**, 7825–7837 (2000).

61. Ohashi M, Kondo T, Ito R, Fukatsu S, Shiraki Y et al. Determination of quadratic nonlinear optical coefficient of $Al_xGa_{1-x}As$ system by the method of reflected second harmonics. *J Appl Phys* **74**, 596–601 (1993).

62. Pernice WHP, Xiong C, Schuck C, Tang HX. Second harmonic generation in phase matched aluminum nitride waveguides and micro-ring resonators. *Appl Phys Lett* **100**, 223501 (2012).

63. Berger V. Second-harmonic generation in monolithic cavities. *J Opt Soc Am B* **14**, 1351–1360 (1997).

64. Liscidini M, Andreani LC. Second-harmonic generation in doubly resonant microcavities with periodic dielectric mirrors. *Phys Rev E* **73**, 016613 (2006).

65. Lalanne P, Yan W, Vynck K, Sauvan C, Hugonin JP. Light interaction with photonic and plasmonic resonances. *Laser Photonics Rev* **12**, 1700113 (2018).

66. Bernhardt N, Koshelev K, White SJU, Meng KWC, Fröch JE et al. Quasi-bic resonant enhancement of second-harmonic generation in WS_2 monolayers. *Nano Lett* **20**, 5309–5314 (2020).

67. Gigli C, Wu T, Marino G, Borne A, Leo G et al. Quasinormal-mode non-hermitian modeling and design in nonlinear nano-optics. *ACS Photonics* **7**, 1197–1205 (2020).

68. Koshelev K, Kruk S, Melik-Gaykazyan E, Choi JH, Bogdanov A et al. Subwavelength dielectric resonators for nonlinear nanophotonics. *Science* **367**, 288–292 (2020).

69. Frizyuk K, Volkovskaya I, Smirnova D, Poddubny A, Petrov M. Second-harmonic generation in mie-resonant dielectric nanoparticles made of noncentrosymmetric materials. *Phys Rev B* **99**, 075425 (2019).

70. Gili VF, Carletti L, Chouchane F, Wang G, Ricolleau C et al. Role of the substrate in monolithic AlGaAs nonlinear nanoantennas. *Nanophotonics* **7**, 517–521 (2017).

71. Balanis CA. *Antenna Theory*: *Analysis and Design* 4th ed (John Wiley & Sons, Hoboken, 2016).

72. Carletti L, Rocco D, Locatelli A, De Angelis C, Gili VF et al. Controlling second-harmonic generation at the nanoscale with monolithic AlGaAs-on-AlOx antennas. *Nanotechnology* **28**, 114005 (2017).

73. Xu L, Rahmani M, Smirnova D, Kamali KZ, Zhang GQ et al. Highly-efficient longitudinal second-harmonic generation from doubly-resonant AlGaAs nanoantennas. *Photonics* **5**, 29 (2018).

74. Xu L, Rahmani M, Kamali KZ, Lamprianidis A, Ghirardini L et al. Boosting third-harmonic generation by a mirror-enhanced anapole resonator. *Light Sci Appl* **7**, 44 (2018).

75. Gili VF, Ghirardini L, Rocco D, Marino G, Favero I et al. Metal-dielectric hybrid nanoantennas for efficient frequency conversion at the anapole mode. *Beilstein J Nanotechnol* **9**, 2306–2314 (2018).

76. Timofeeva M, Lang L, Timpu F, Renaut C, Bouravleuv A et al. Anapoles in free-standing III-V nanodisks enhancing second-harmonic generation. *Nano Lett* **18**, 3695–3702 (2018).

77. Semmlinger M, Zhang M, Tseng ML, Huang TT, Yang J et al. Generating third harmonic vacuum ultraviolet light with a TiO_2 metasurface. *Nano Lett* **19**, 8972–8978 (2019).

78. Carletti L, Koshelev K, De Angelis C, Kivshar Y. Giant nonlinear response at the nanoscale driven by bound states in the continuum. *Phys Rev Lett* **121**, 033903 (2018).

79. Volkovskaya I, Xu L, Huang LJ, Smirnov AI, Miroshnichenko AE et al. Multipolar second-harmonic generation from high-Q quasi-BIC states in subwavelength resonators. *Nanophotonics* **9**, 3953–3963 (2020).

80. Carletti L, Locatelli A, Neshev D, De Angelis C. Shaping the radiation pattern of second-harmonic generation from AlGaAs dielectric nanoantennas. *ACS Photonics* **3**, 1500–1507 (2016).

81. Ghirardini L, Marino G, Gili VF, Favero I, Rocco D et al. Shaping the nonlinear emission pattern of a dielectric nanoantenna by integrated holographic gratings. *Nano Lett* **18**, 6750–6755 (2018).

82. Xu L, Saerens G, Timofeeva M, Smirnova DA, Volkovskaya I et al. Forward and backward switching of nonlinear unidirectional emission from GaAs nanoantennas. *ACS Nano* **14**, 1379–1389 (2020).

83. Saerens G, Tang I, Petrov MI, Frizyuk K, Renaut C et al. Engineering of the second-harmonic emission directionality with III–V semiconductor rod nanoantennas. *Laser Photonics Rev* **14**, 2000028 (2020).

84. Rocco D, Gigli C, Carletti L, Marino G, Vincenti MA et al. Vertical second harmonic generation in asymmetric dielectric nanoantennas. *IEEE Photonics J* **12**, 4500507 (2020).

85. Sautter JD, Xu L, Miroshnichenko AE, Lysevych M, Volkovskaya I et al. Tailoring second-harmonic emission from (111)-GaAs nanoantennas. *Nano Lett* **19**, 3905–3911 (2019).

86. Ghirardini L, Carletti L, Gili V, Pellegrini G, Duò L et al. Polarization properties of second-harmonic generation in AlGaAs optical nanoantennas. *Opt Lett* **42**, 559–562 (2017).

87. Kruk SS, Camacho-Morales R, Xu L, Rahmani M, Smirnova DA et al. Nonlinear optical magnetism revealed by second-harmonic generation in nanoantennas. *Nano Lett* **17**, 3914–3918 (2017).

88. Zou SL, Schatz GC. Theoretical studies of plasmon resonances in one-dimensional nanoparticle chains: narrow lineshapes with tunable widths. *Nanotechnology* **17**, 2813–2820 (2006).

89. Evlyukhin AB, Reinhardt C, Seidel A, Luk'yanchuk BS, Chichkov BN. Optical response features of Si-nanoparticle arrays. *Phys Rev B* **82**, 045404 (2010).

90. Kravets VG, Kabashin AV, Barnes WL, Grigorenko AN. Plasmonic surface lattice resonances: a review of properties and applications. *Chem Rev* **118**, 5912–5951 (2018).

91. Castellanos GW, Bai P, Rivas JG. Lattice resonances in dielectric metasurfaces. *J Appl Phys* **125**, 213105 (2019).

92. Babicheva VE, Evlyukhin AB. Multipole lattice effects in high refractive index metasurfaces. *J Appl Phys* **129**, 040902 (2021).

93. Vincent Vinel, Zejian Li, Adrien Borne, Adrien Bensemhoun, Ivan Favero et al. Non-Hermitian bath model for arrays of coupled nanoresonators. *Opt Express* **29**, 34015–34023 (2021).

94. Rybin MV, Limonov MF. Resonance effects in photonic crystals and metamaterials: (100th anniversary of the ioffe institute). *Phys-Usp* **62**, 823–838 (2019).

95. Grahn P, Shevchenko A, Kaivola M. Electromagnetic multipole theory for optical nanomaterials. *New J Phys* **14**, 093033 (2012).

96. Liu S, Vabishchevich PP, Vaskin A, Reno JL, Keeler GA et al. An all-dielectric metasurface as a broadband optical frequency mixer. *Nat Commun* **9**, 2507 (2018).

97. Semmlinger M, Tseng ML, Yang J, Zhang M, Zhang C et al. Vacuum ultraviolet light-generating metasurface. *Nano Lett* **18**, 5738–5743 (2018).

98. Löchner FJF, Fedotova AN, Liu S, Keeler GA, Peake GM et al. Polarization-dependent second harmonic diffraction from resonant GaAs metasurfaces. *ACS Photonics* **5**, 1786–1793 (2018).

99. Marino G, Gigli C, Rocco D, Lemaître A, Favero I et al. Zero-order second harmonic generation from AlGaAs-on-insulator metasurfaces. *ACS Photonics* **6**, 1226–1231 (2019).

100. Gigli C, Marino G, Suffit S, Patriarche G, Beaudoin G et al. Polarization- and diffraction-controlled second-harmonic generation from semiconductor metasurfaces. *J Opt Soc Am B* **36**, E55–E64 (2019).

101. Carletti L, Zilli A, Moia F, Toma A, Finazzi M et al. Steering and encoding the polarization of the second harmonic in the visible with a monolithic $LiNbO_3$ metasurface. *ACS Photonics* **8**, 731–737 (2021).

102. Carletti L, Li C, Sautter J, Staude I, De Angelis C et al. Second harmonic generation in monolithic lithium niobate metasurfaces. *Opt Express* **27**, 33391–33398 (2019).

103. Frizyuk K. Second-harmonic generation in dielectric nanoparticles with different symmetries. *J Opt Soc Am B* **36**, F32–F37 (2019).

104. Gigli C, Li QT, Chavel P, Leo G, Brongersma ML et al. Fundamental limitations of huygens' metasurfaces for optical beam shaping. *Laser Photonics Rev* **15**, 2000448 (2021).

105. Li GX, Chen SM, Pholchai N, Reineke B, Wong PWH et al. Continuous control of the nonlinearity phase for harmonic generations. *Nat Mater* **14**, 607–612 (2015).

106. Wang L, Kruk S, Koshelev K, Kravchenko I, Luther-Davies B et al. Nonlinear wavefront control with all-dielectric metasurfaces. *Nano Lett* **18**, 3978–3984 (2018).

107. Schlickriede C, Kruk SS, Wang L, Sain B, Kivshar Y et al. Nonlinear imaging with all-dielectric metasurfaces. *Nano Lett* **20**, 4370–4376 (2020).

108. Gigli C, Marino G, Artioli A, Rocco D, De Angelis C et al. Tensorial phase control in nonlinear meta-optics. *Optica* **8**, 269–276 (2021).

109. Bar-David J, Levy U. Nonlinear diffraction in asymmetric dielectric metasurfaces. *Nano Lett* **19**, 1044–1051 (2019).

110. Yu NF, Genevet P, Kats MA, Aieta F, Tetienne JP et al. Light propagation with phase discontinuities: generalized laws of reflection and refraction. *Science* **334**, 333–337 (2011).

111. Aieta F, Genevet P, Kats MA, Yu NF, Blanchard R et al. Aberration-free ultrathin flat lenses and axicons at telecom wavelengths based on plasmonic metasurfaces. *Nano Lett* **12**, 4932–4936 (2012).

112. Almeida E, Bitton O, Prior Y. Nonlinear metamaterials for holography. *Nat Commun* **7**, 12533 (2016).

113. Almeida E, Shalem G, Prior Y. Subwavelength nonlinear phase control and anomalous phase matching in plasmonic metasurfaces. *Nat Commun* **7**, 10367 (2016).

114. Schlickriede C, Waterman N, Reineke B, Georgi P, Li GX et al. Imaging through nonlinear metalens using second harmonic generation. *Adv Mater* **30**, 1703843 (2018).

115. Ye WM, Zeuner F, Li X, Reineke B, He S et al. Spin and wavelength multiplexed nonlinear metasurface holography. *Nat Commun* **7**, 11930 (2016).

116. Walter F, Li GX, Meier C, Zhang S, Zentgraf T. Ultrathin nonlinear metasurface for optical image encoding. *Nano Lett* **17**, 3171–3175 (2017).

117. Reineke B, Sain B, Zhao RZ, Carletti L, Liu BY et al. Silicon metasurfaces for third harmonic geometric phase manipulation and multiplexed holography. *Nano Lett* **19**, 6585–6591 (2019).

118. Dasgupta A, Gao J, Yang XD. Second-harmonic optical vortex conversion from WS_2 monolayer. *Sci Rep* **9**, 8780 (2019).

119. Hu GW, Hong XM, Wang K, Wu J, Xu HX et al. Coherent steering of nonlinear chiral valley photons with a synthetic Au–WS_2 metasurface. *Nat Photonics* **13**, 467–472 (2019).

120. Powell DA. Interference between the modes of an all-dielectric meta-atom. *Phys Rev Appl* **7**, 034006 (2017).

121. Yang YM, Wang WY, Boulesbaa A, Kravchenko II, Briggs DP et al. Nonlinear fano-resonant dielectric metasurfaces. *Nano Lett* **15**, 7388–7393 (2015).

122. Liu HZ, Guo C, Vampa G, Zhang JL, Sarmiento T et al. Enhanced high-harmonic generation from an all-dielectric metasurface. *Nat Phys* **14**, 1006–1010 (2018).

123. Huang ZJ, Lu HH, Xiong HQ, Li Y, Chen HJ et al. Fano resonance on nanostructured lithium niobate for highly efficient and tunable second harmonic generation. *Nanomaterials* **9**, 69 (2019).

124. Vabishchevich PP, Liu S, Sinclair MB, Keeler GA, Peake GM et al. Enhanced second-harmonic generation using broken symmetry III-V semiconductor fano metasurfaces. *ACS Photonics* **5**, 1685–1690 (2018).

125. Koshelev K, Tang YT, Li KF, Choi DY, Li GX et al. Nonlinear metasurfaces governed by bound states in the continuum. *ACS Photonics* **6**, 1639–1644 (2019).

126. Liu ZJ, Xu Y, Lin Y, Xiang J, Feng TH et al. High- *Q* quasi-bound states in the continuum for nonlinear metasurfaces. *Phys Rev Lett* **123**, 253901 (2019).

127. Anthur AP, Zhang HZ, Paniagua-Dominguez R, Kalashnikov DA, Ha ST et al. Continuous wave second harmonic generation enabled by quasi-bound-states in the continuum on gallium phosphide metasurfaces. *Nano Lett* **20**, 8745–8751 (2020).

128. Fan SH, Joannopoulos JD. Analysis of guided resonances in photonic crystal slabs. *Phys Rev B* **65**, 235112 (2002).

129. Lalanne P, Hugonin JP, Chavel P. Optical properties of deep lamellar gratings: a coupled bloch-mode insight. *J Light Technol* **24**, 2442–2449 (2006).

130. Hsu CW, Zhen B, Stone AD, Joannopoulos JD, Soljačić M. Bound states in the continuum. *Nat Rev Mater* **1**, 16048 (2016).

131. Koshelev K, Lepeshov S, Liu MK, Bogdanov A, Kivshar Y. Asymmetric metasurfaces with high-Q resonances governed by bound states in the continuum. *Phys Rev Lett* **121**, 193903 (2018).

132. Campione S, Liu S, Basilio LI, Warne LK, Langston WL et al. Broken symmetry dielectric resonators for high quality factor fano metasurfaces. *ACS Photonics* **3**, 2362–2367 (2016).

133. Tong WY, Gong C, Liu XJ, Yuan S, Huang QZ et al. Enhanced third harmonic generation in a silicon metasurface using trapped mode. *Opt Express* **24**, 19661–19670 (2016).

134. Löchner FJF, George A, Koshelev K, Bucher T, Najafidehaghani E et al. Hybrid dielectric metasurfaces for enhancing second-harmonic generation in chemical vapor deposition grown MoS_2 monolayers. *ACS Photonics* **8**, 218–227 (2021).

135. Scaccabarozzi L, Fejer MM, Huo YJ, Fan SH, Yu XJ et al. Enhanced second-harmonic generation in AlGaAs/Al$_x$O$_y$ tightly confining waveguides and resonant cavities. *Opt Lett* **31**, 3626–3628 (2006).

136. Guo X, Zou CL, Tang HX. Second-harmonic generation in aluminum nitride microrings with 2500%/W conversion efficiency. *Optica* **3**, 1126–1131 (2016).

137. Bruch AW, Liu XW, Guo X, Surya JB, Gong Z et al. 17 000%/W second-harmonic conversion efficiency in single-crystalline aluminum nitride microresonators. *Appl Phys Lett* **113**, 131102 (2018).

138. Lu JJ, Surya JB, Liu XW, Bruch AW, Gong Z et al. Periodically poled thin-film lithium niobate microring resonators with a second-harmonic generation efficiency of 250, 000%/W. *Optica* **6**, 1455–1460 (2019).

139. Ilchenko VS, Savchenkov AA, Matsko AB, Maleki L. Nonlinear optics and crystalline whispering gallery mode cavities. *Phys Rev Lett* **92**, 043903 (2004).

140. Fürst JU, Strekalov DV, Elser D, Lassen M, Andersen UL et al. Naturally phase-matched second-harmonic generation in a whispering-gallery-mode resonator. *Phys Rev Lett* **104**, 153901 (2010).

141. Mariani S, Andronico A, Lemaître A, Favero I, Ducci S et al. Second-harmonic generation in AlGaAs microdisks in the telecom range. *Opt Lett* **39**, 3062–3065 (2014).

142. Kuo PS, Bravo-Abad J Solomon GS. Second-harmonic generation using-quasi-phasematching in a GaAs whispering-gallery-mode microcavity. *Nat Commun* **5**, 3109 (2014).

143. Wang C, Burek MJ, Lin Z, Atikian HA, Venkataraman V et al. Integrated high quality factor lithium niobate microdisk resonators. *Opt Express* **22**, 30924–30933 (2014).

144. Lin JT, Xu YX, Ni JL, Wang M, Fang ZW et al. Phase-matched second-harmonic generation in an on-chip LiNbO$_3$ microresonator. *Phys Rev Appl* **6**, 014002 (2016).

145. Corcoran B, Monat C, Grillet C, Moss DJ, Eggleton BJ et al. Green light emission in silicon through slow-light enhanced third-harmonic generation in photonic-crystal waveguides. *Nat Photonics* **3**, 206–210 (2009).

146. Galli M, Gerace D, Welna K, Krauss TF, O'Faolain L et al. Low-power continuous-wave generation of visible harmonics in silicon photonic crystal nanocavities. *Opt Express* **18**, 26613–26624 (2010).

147. Rivoire K, Lin ZL, Hatami F, Masselink WT, Vučković J. Second harmonic generation in gallium phosphide photonic crystal nanocavities with ultralow continuous wave pump power. *Opt Express* **17**, 22609–22615 (2009).

148. Diziain S, Geiss R, Zilk M, Schrempel F, Kley EB et al. Second harmonic generation in free-standing lithium niobate photonic crystal L3 cavity. *Appl Phys Lett* **103**, 051117 (2013).

149. Yamada S, Song BS, Jeon S, Upham J, Tanaka Y et al. Second-harmonic generation in a silicon-carbide-based photonic crystal nanocavity. *Opt Lett* **39**, 1768–1771 (2014).

150. Mohamed MS, Simbula A, Carlin JF, Minkov M, Gerace D et al. Efficient continuous-wave nonlinear frequency conversion in high-Q gallium nitride photonic crystal cavities on silicon. *APL Photonics* **2**, 031301 (2017).

151. Buckley S, Radulaski M, Petykiewicz J, Lagoudakis KG, Kang JH et al. Second-harmonic generation in GaAs photonic crystal cavities in (111)B and (001) crystal orientations. *ACS Photonics* **1**, 516–523 (2014).

152. Minkov M, Gerace D, Fan SH. Doubly resonant $\chi^{(2)}$ nonlinear photonic crystal cavity based on a bound state in the continuum. *Optica* **6**, 1039–1045 (2019).

153. Wang J, Clementi M, Minkov M, Barone A, Carlin JF et al. Doubly resonant second-harmonic generation of a vortex beam from a bound state in the continuum. *Optica* **7**, 1126–1132 (2020).

154. Seghilani MS, Myara M, Sellahi M, Legratiet L, Sagnes I et al. Vortex Laser based on III-V semiconductor metasurface: direct generation of coherent laguerre-gauss modes carrying controlled orbital angular momentum. *Sci Rep* **6**, 38156 (2016).

155. Shcherbakov MR, Vabishchevich PP, Shorokhov AS, Chong KE, Choi DY et al. Ultrafast all-optical switching with magnetic resonances in nonlinear dielectric nanostructures. *Nano Lett* **15**, 6985–6990 (2015).

156. Rocco D, Carletti L, Caputo R, Finazzi M, Celebrano M et al. Switching the second harmonic generation by a dielectric metasurface via tunable liquid crystal. *Opt Express* **28**, 12037–12046 (2020).

157. Baranov DG, Zuev DA, Lepeshov SI, Kotov OV, Krasnok AE et al. All-dielectric nanophotonics: the quest for better materials and fabrication techniques. *Optica* **4**, 814–825 (2017).

158. Makarov SV, Zalogina AS, Tajik M, Zuev DA, Rybin MV et al. Light-induced tuning and reconfiguration of nanophotonic structures. *Laser Photonics Rev* **11**, 1700108 (2017).

159. Shcherbakov MR, Eilenberger F, Staude I. Interaction of semiconductor metasurfaces with short laser pulses: from nonlinear-optical response toward spatiotemporal shaping. *J Appl Phys* **126**, 085705 (2019).

160. Keren-Zur S, Michaeli L, Suchowski H, Ellenbogen T. Shaping light with nonlinear metasurfaces. *Adv Opt Photonics* **10**, 309–353 (2018).

161. Gao H, Fan XH, Xiong W, Hong MH. Recent advances in optical dynamic meta-holography. *Opto-Electron Adv* **4**, 210030 (2021).

162. Smirnova D, Smirnov AI, Kivshar YS. Multipolar second-harmonic generation by Mie-resonant dielectric nanoparticles. *Phys Rev A* **97**, 013807 (2018).

163. Elsawy MMR, Lanteri S, Duvigneau R, Fan JA, Genevet P. Numerical optimization methods for metasurfaces. *Laser Photonics Rev* **14**, 1900445 (2020).

Acknowledgements

Competing interests

The authors declare no competing financial interests.